Master's Thesis

Conductivity Gradient Lithium Hosts based on Hetero-fibrous Scaffolds for Lithium-Metal Batteries

Sang-Ho Hong

Department of Energy Engineering
(Battery Science and Technology)

Graduate School of UNIST

2019

Conductivity Gradient Lithium Hosts based on Hetero-Fibrous Scaffolds for Lithium-Metal Batteries

Sang-Ho Hong

Department of Energy Engineering
(Battery Science and Technology)

Graduate School of UNIST

Conductivity Gradient Lithium Hosts based on Hetero-Fibrous Scaffolds for Lithium-Metal Batteries

A thesis/dissertation
submitted to the Graduate School of UNIST
in partial fulfillment of the
requirements for the degree of

Master of Science

Sang-Ho Hong

12/10/2018 Month/Day/Year of submission
Approved by

Advisor: Sang-Young Lee

Conductivity Gradient Lithium Hosts based on Hetero-fibrous Scaffolds for Lithium-Metal Batteries

Sang-Ho Hong

This certifies that the thesis/dissertation of Sang-Ho Hong is approved.

12/10/2018 Month/Day/Year of submission

signature

Advisor: Sang-Young Lee

signature

Seok Ju Kang

signature

Hyun-Wook Lee

Contents

Abstract ····· 1

List of figures ····· 2

List of tables ····· 4

I. Introduction ····· 5

1.1. Operation principle to lithium ion batteries ····· 5

1.2. General requirements of a negative electrode for lithium ion batteries ····· 7

II. Conductivity Gradient Lithium Hosts based on Hetero-Fibrous Scaffolds for Lithium-Metal Batteries ····· 10

2.1. Introduction ····· 10

2.2. Experimental ····· 13

2.2.1. Simulation method ····· 13

2.2.2. Fabrication of electronic conductivity gradient host ····· 13

2.2.3. Structural/physicochemical characterization ····· 14

2.2.4. Electrochemical measurements ····· 14

2.3. Results and discussion ····· 16

2.3.1. Demonstration of electronic conductivity gradient effect ····· 16

2.3.2. Characterization of electronic conductivity gradient Li host ····· 18

2.3.3. Influence on Li protection and plating/stripping behavior ····· 24

2.3.4. Electrochemical performance of electronic conductivity gradient host ····· 31

2.4. Conclusion ····· 39

III. References ····· 40

Abstract

Metallic lithium (Li) have attracted considerable attention owing to its high theoretical capacity (3860 mAh g^{-1}) as a promising anode candidate for next-generation battery. However, uneven plating/stripping behaviors of Li metal leads to severe safety issues and poor cycling performance due to formation of dendritic Li, seriously impeding the practical Li metal-based batteries. Here, we demonstrate a newly designed Li metal host (Li host) based on hetero-fibrous scaffold composed of one-dimensional (1D) electronic conductor (copper nanowire, CuNW) and electronic insulator (cellulose nanofiber, CNF) with electronic conductivity gradient structure. The electronic conductivity gradient architecture in the new scaffold offers stable Li plating/stripping behaviors which form preferential and uniformly dense Li deposition on the bottom layer with high electronic conductivity and suppression of Li dendritic growth on top surface of non-conductive top layer. Additionally, the middle layer which has well-tailored electronic conductivity enable effectively suppression dead Li formed from bottom layer and support to enhance actualization of long-term cyclability. These featured structural characteristics of Li host with electronic conductivity gradient achieve high Li utilization (>96% coulombic efficiency) and superior cycling stability at the current density of 1 mA cm^{-2} over 250 cycles. The resultant of NCM811||Li@host full-cell shows excellent cycling performance and structural stability of anode, thus demonstrating proper as Li host for high-energy density Li metal batteries.

List of figures

Figure 1.1. A schematic diagram of Li-ion batteries composed of graphite (Li_xC_6) as a negative electrode and $LiMO_2$ (lithium metal oxide) as a positive electrode.

Figure 2.1. Conceptual illustration and COMSOL Multiphysics of Li plating on (a) Cu foil, (b) Cu Mesh and (c) CG host.

Figure 2.2. Fabrication and characteristics of CG host. (a) Schematic representation and photographs (insets) demonstrating the fabrication and the structural robustness of CG host. (b) SEM image for the cross-section view of CG host. SEM image of the surface view for each layer (c) bottom layer (CuNW) (d) middle layer (CuNW@CNF) (e) top layer (CNF@SiO_2).

Figure 2.3. Characterization of the electronic conductivity gradient host via elemental EDX spectrum. Morphology of each layer highlighted with different colors in the cross-section SEM image of CG host. The inset SEM images and corresponding elemental EDX spectrum of (a) top layer (CNF@SiO_2), (b) middle layer (CuNW@CNF) and (c) bottom layer (CuNW)

Figure 2.4. Electronic characterization of the CuNW before and after annealing. (a) XPS spectrum of the CuNW before and after annealing. Photographs of the multi-meter measurement for CuNW (b) before and (c) after annealing process.

Figure 2.5. The Li plating/stripping behavior on/from the CG host in detail via SEM images. (a) Li plating/stripping states in the galvanostatic discharge/charge voltage profile at 3 mA cm^{-2}. The cross-section view SEM images of (b) the pristine CG host (DOC 0%) and after Li plating (c) 3 mAh cm^{-2} (DOC 42%) (d) 7 mAh cm^{-2} (DOC 100%). SEM images CG Host after stripping (e) 2 mAh cm^{-2} (DOC 71%), (f) 7 mAh cm^{-2} (DOC 0%).

Figure 2.6. Surface morphology and photographs after 20 cycles of Li plating/stripping at 0.5 mA cm^{-2} on (a) Cu foil and CG host (b) without and (c) with thin (1 μm) and (d) thick (10 μm) top layer (CNF@SiO_2).

Figure 2.7. Optimization of CG host structure for stable Li plating/stripping. (a) and (b) Thickness of top layer (CNF@SiO_2). (c) and (d) Electronic conductivity difference between middle (CuNW@CNF) and bottom layer (CuNW).

Figure 2.8. Electrochemical performance in cells with different Li host. (a) Galvanostatic Li plating/stripping voltage profile for the Li||Li@host symmetric cell using Cu foil, CuNW and CG host at 1 mA cm^{-2} for 1 mAh cm^{-2} and (b) Comparison of the Coulombic efficiency for Li||host asymmetric cell using Cu foil, CuNW and CG host at 0.5 mA cm^{-2} for 1 mAh cm^{-2}. (c) Cycling performance of the NCM811 full-cell using Cu foil and CG host at 1 C (d) Surface morphology on CG host after 100 cycles of NCM811||Li@host full-cell

Figure 2.9. Voltage profiles of Li plating/stripping on (a) Cu foil and (b) CG host with current density of 1 mA cm^{-2} for 1 mAh cm^{-2}.

Figure 2.10. Impedance spectra study of the CG host electrode for Li plating/stripping at 1 mA cm^{-2}. (a) The corresponding equivalent circuit model. Impedance spectra for the cell using (b) Cu foil and (c) CG host

Figure 2.11. Voltage profiles for NCM811||Li@host for (a) Cu foil and (b) CG host under 1C.

Figure 2.12. Surface morphology of Cu foil after 100 cycles of NCM811||Li@host full-cell.

List of tables

Table 1.1. Most common anode materials for lithium ion batteries.

Table 1.2. Popular commercial anode material in lithium ion batteries.

Table 2.1. Textural parameters of each layer in the electronic conductivity gradient host (CG Host).

Table 2.2. Electronic parameters of middle (CuNW@CNF) layer depending on different composition of CuNW and CNF.

Table 2.3. Summary of representative papers about electrolyte design for Li metal batteries.

I. Introduction

1.1. Operation principle to lithium ion batteries

As major energy storage system, the lithium-ion batteries (LiBs) have attracted much attention from a various industry fields as a commercial energy storage for electric vehicles (EVs), portable electronics and large-scale electrical grids. The lithium-ion batteries are basically required stable electrochemical characteristics and strong safety endurance. Because the lithium-ion batteries have still severe hurdle regarding safety issues of cells and the electrochemical performance degradation.

Basically, an integrated lithium-ion batteries consist of four part, an anode (negative electrode), an electrolyte, separator and a cathode (positive electrode) (Figure 1). And the two electrodes should be separated by a porous polymer membrane with swelled in a mixture of solvents and salts. In the charge/discharge step, lithium ions are move out and in the interstitial void between atomic layers in the cathode. In detail, on charging state of the battery, Li-ions coming from a cathode (positive electrode) transfer through electrolyte-filled channels in separator to an anode (negative electrode) and the electrons simultaneously move through the external circuit (Equation 1). In contrast, on discharging state of the battery the above reaction occurs reversely (Equation 2).[1]

$$\text{Anode side:} \quad xLi^+ + xe^- + xC_6 \rightleftarrows xLiC_6 \quad (1)$$

$$\text{Cathode side:} \quad LiMO_2 \rightleftarrows Li_{1-x}MO_2 + xLi^+ + xe^- \quad (2)$$

$$\text{Total reaction:} \quad xC_6 + LiMO_2 \rightleftarrows Li_{1-x}MO_2 + xLiC \quad (3)$$

(→: Charge reaction, ←: Discharge reaction)

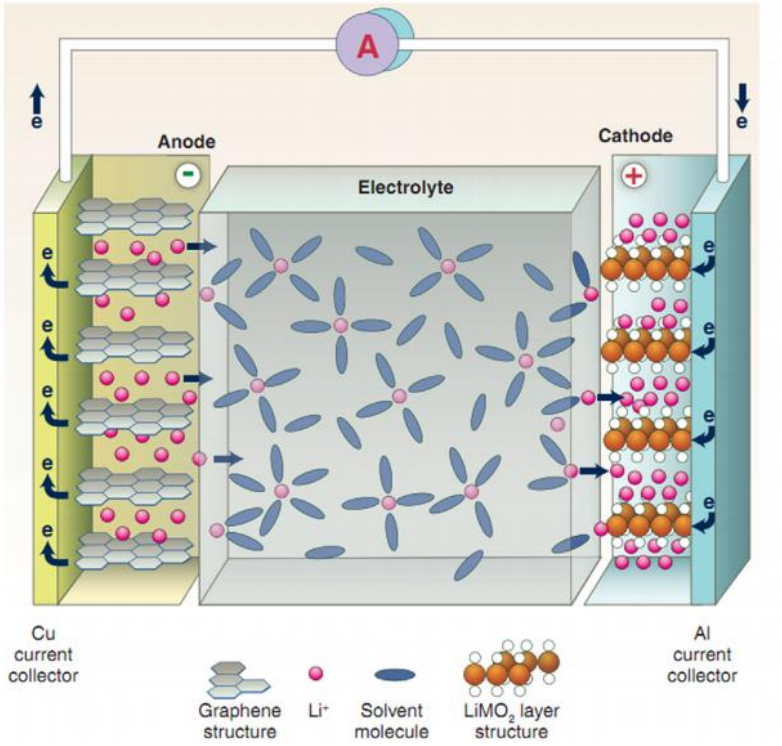

Figure 1.1. A schematic diagram of Li-ion batteries composed of graphite (Li_xC_6) as a negative electrode and $LiMO_2$ (lithium metal oxide) as a positive electrode.

1.2. General requirements of a negative electrode for lithium ion batteries

The negative electrode in the infancy for battery industry was used lithium metal due to its high theoretical capacity (3860 mAh g-1) and lowest redox potential (-3.04 V vs. the standard hydrogen electrode). However, during charging and discharging state, lithium dendrite grows up and it leads to short-circuit of the batteries and safety issues. For substitute of lithium metal as anode, silicon, zinc and so forth are tried to solve the dendritic growth problem. Nevertheless, the alloy form anode has a problem of capacity dropping down quickly after a few of charge/discharge cycles because of the volume expansion resulted from huge stress in the alloy crystal lattice. Alternatively, Sony Corporation developed the highly reversible carbonaceous material with the low voltage anode. And they succeeded in commercializing the rocking chair cells with the carbon anode and $LiCoO_2$ cathode in the early 1990s.[2]

The various of layer-structured carbon as anode could accommodate of lithium ion inserting into the layered structure and keep the very stable state, it shows the path of the possibility for solving the safety issues due to growth of dendritic lithium. In addition, the layer-structured carbon offers a slight structural change during insertion and extraction of lithium ion and achieve a base to realize high capacity and excellent cyclability of lithium ion batteries with highly stable oxidation/reduction reaction. Basically, the electrochemical performance for lithium ion batteries is also affected by a negative electrode. For maximizing the electrochemical performance of lithium ion batteries, the following requirements is essential for a negative electrode for lithium ion batteries; i) the negative electrode should have the low redox potential for the high voltage of the assembled cell with a cathode. ii) The strong structural stability should be required during the insertion/extraction of lithium ion for high reversibility of lithium ion and durable cyclability. iii) the high reaction reversibility is also essential for an ideal coulombic efficiency that means there is no capacity decay according to cycle number. iv) the lithium ion diffusion kinetics and v) high electron conductivity in the negative electrode is important for high performance lithium ion batteries. Lastly, for the high energy density anode, the ideal anode should have high density. Generally, the graphite has theoretical density is 2.2 g/ml and has 818 mAh/ml theoretical volumetric capacity density.[2]

The intrinsic properties of the anode materials are determined the electrochemical performance for lithium ion batteries. Table 1.1-1.2 present the properties of the various materials as a negative electrode.

Table 1.1. Most common anode materials for lithium ion batteries.[3]

Anode material	Theoretical capacity	Advantage	Common issues
insertion/de-insertion materials			
Hard carbons	200-600	Good working potential Low cost Good safety	Low coulomb efficiency High voltage hysteresis High irreversible capacity
CNTS	1116		
Graphene	780/1116		
$LiTi_4O_5$	175	Extreme safety Good cycle life Low cost High power capability	Very low capacity Low energy density
TiO_2	330		
Alloy/de-alloy materials			
Silicon	4212	Higher specific capacities High energy density Good safety	Large irreversible capacity Huge capacity fading Poor cycling
Germanium	1624		
Tin	993		
Antimony	660		
Tin oxide	790		
SiO	1600		
Conversion materials			
Metal oxides	500-1200	High capacity High energy Low cost Environmentally compatibility High specific capacity Low operation potential and low polarization than counter oxides	Low coulombic efficiency Unstable SEI formation Large potential hysteresis Poor cycle life Poor capacity retention Short cycle life High cost of production
Metal phoshides/sulfides /nitrides	500-1800		

Table 2.2. Popular commercial anode material in lithium ion batteries.[4]

Anode material	Company	Capacity	Nominal Voltage (V)	Specific Energy	Cycle Life
Tin based Amorphous Material	Sony	900 mAh	4.2-2.5	158 Wh kg^{-1}	-
$Li_4Ti_5O_{12}$	Toshiba	40 Ah	27.6 (18-32.4)	79 Wh kg^{-1}	10000
		20 Ah	2.3 (1.5-2.7)	177 Wh L^{-1}	10000
Si-C	Envia	40 Ah	3.74	215 Wh kg^{-1}	>1000
		27 Ah	3.74	184 Wh kg^{-1}	5000
Si@SiO_2 core@shell	Amprius	1566 Ah kg^{-1}	-	-	6000

II. Conductivity Gradient Lithium Hosts based on Hetero-fibrous Scaffolds for Lithium-Metal Batteries

2.1. Introduction

The global energy crisis and environmental aggravation have facilitated the development of green power source technologies, it in turn has encouraged considerable attention to energy storage system including lithium-ion batteries (LiBs).[5,6] In the prospective ubiquitous energy era, which will find worldwide application of electrical transportation, the Internet of Things (IoT) and large-scale energy storage system, the relentless demand of superior energy storage with high energy density, electrochemical stability will be essentially required.[7-10] However, although we have witnessed the massive development in lithium-ion batteries, the theoretical specific energy density (~ 350 Wh kg^{-1}) of conventional lithium-ion batteries using graphite anode cannot meet the ever-increasing demand in the ubiquitous energy era. Therefore, an energy storage system beyond lithium-ion batteries are need to able for commercial high energy density rechargeable batteries.[11,12]

The one of the most promising alternatives is the energy storage system using metallic lithium (Li) as anode for next generation rechargeable batteries, especially Li-S, Li-air and lithium metal battery (LMB) systems. Because lithium metal has the highest theoretical capacity (3,860 mAh g^{-1}), lowest electrochemical potential (-3.04 V vs. the standard hydrogen electrode) and low density (0.534 g cm^{-3}), leading to a promising anode candidate for high energy density rechargeable batteries.[13,14] Despite these attractive advantages, lithium metal has several remaining hurdles in the energy storage systems using lithium metal as anode. During repeated lithium plating and stripping processes, unmanageable lithium dendritic growth due to uneven lithium ion flux and solid electrolyte interphase (SEI) leads to generate thick SEI layers, increase the internal resistance and continuously consume lithium metal and electrolyte with huge volume expansion resulted from host-less nature. As a result of it, poor cycle life and even serious safety hazard including explosion of the cell due to internal short-circuits could be occur, thus these challenges must be solved prior to the development of the commercial application of lithium metal anode.[11,12,15]

For several decades, the soaring attentions in lithium metal battery systems has facilitated innumerable efforts for addressing the issues of the lithium dendritic growth. The optimizing electrolyte components or additives for reinforcing stability of SEI layer between electrolyte and lithium metal anode have been investigated.[16-19] In addition, a modified artificial SEI layer as protective layer have been employed to effectively prevent dendrite propagation.[20-24] One method is to suppress lithium dendrite penetration by using solid-state electrolyte with high modulus. All of strategies have proved being effective for improving SEI stability and suppressing lithium dendrite growth. In these numerous studies, designing the nanoarchitecture of the lithium metal or lithium host framework with high surface

area offers attractive properties such as low local density by increasing electrochemical active area and accommodation of volume expansion during repeated cycle processes.[25-32]

Uniform confinement of lithium within the host framework is indispensable for conserving a stable electrode dimension and blocking occurrence of 'dead Li' as reported in prior studies.[30,33,34] However, because the electric field in the sandwich cell construction is mainly formed vertically, thus the direct lithium nucleation and dendritic growth on the top surface still should take place in conventional lithium host framework due to high electronic conductivity of the top surface, Recently, for solving the issue of top surface lithium nucleation, modulating the direction of the lithium growth to the lateral direction was employed and proved improvement of cyclability.[35] The other method is selective lithium deposition into inner space of host by using lithiophilic material as a lithium nucleation seed on the lithium host and it offers blocking the exposure of deposited lithium and stable cyclability.[36,37] However, the reported lithium hosts have limitation of operation at high current density due to their high electronic conductivity of top surface or too high thickness in terms of energy density. Therefore, to enable a lithium metal battery to work at high current density and achieve high energy density lithium metal battery, a comparatively thin thickness and even ideal unique structure of lithium host which can suppress the lithium plating on the top surface is imperative.

Herein, we report a new designed of lithium host (Hetero-fibrous scaffold-based conductivity gradient hosts, CG hosts) with electronic conductivity gradient structure based on hetero-fibrous scaffold composed of one-dimensional (1D) electronic conductor (Copper nanowire, CuNW) and insulator (cellulose nanofiber, CNF) as an effective strategy to enable to suppress the lithium plating on top surface and realize the high energy density lithium metal battery. Copper nanowires (CuNWs) as 1D electronic conductor could be easily formed to 3D conductive network and the naturally abundant 1D electronic insulator, cellulose nanofibers (CNFs), can offer structural flexibility in the nanocellulose scaffold with its high mechanical flexibility, it leads to realization of robust hetero-fibrous tri-layered CG host with electronic conductivity gradient structure.

The hetero-fibrous tri-layered CG host has electronic conductivity gradient geometry which is increase the electronic conductivity into the thickness direction from top surface and simultaneously delivers to facilitate an ion transport through well-developed porous structure. Additionally, the nanofibrous scaffold with the intermingled network between the fibrous 1D building blocks ensures robust structural stability. In terms of electronic conductivity, the bottom layer (CuNW) with high electronic conductivity enhances the uniform and dense lithium deposition onto it. And the middle layer (CuNW @CNF) with well-tailored electronic conductivity could support to capture the 'dead Li' and extend cycle life.[37] The top layer (CNF@ SiO_2) as electronic non-conductive layer blocks to plate lithium on the top surface, furthermore the high polarity of CNF and SiO_2 particles, which is the

disassemble-agent for evolution of porous layer,[39] offers good electrolyte wettability leading to expect to uniform lithium-ion flux and additionally support suppression of lithium dendrite.[40.41]

Benefiting from the structural uniqueness and chemical functionality described above, the hetero-fibrous CG host achieves reversible lithium plating/stripping behavior from bottom layer of the host and improvement of cycling performance at high current density, furthermore, the stable cycling performance of full-cell assembled with NCM811 cathode demonstrates the strategy to be successful in the lithium metal full-cell and its cell-based energy density simultaneously reach the highest value in the previous lithium host literatures, to the best of our knowledge.

2.2. Experimental

2.2.1. Simulation method

Our simulations were carried out using COMSOL Multiphysics software. We utilized the tertiary Nernest-Plank interface to model the electrodeposition process in this study. As a model system, we choose a rectangular electrolyte cell filled with 1M LiTFSI in DOL/DME of width and height of 31 × 30 μm^2 and various control electrodes with nanochannels. The material parameters used in the simulations, such as the molar mass, volumetric mass density, cathodic and anodic charge transfer coefficients, and stoichiometric coefficient, correspond to 1M LiTFSI in DOL/DME. The electrode conductivities were considered by applying the boundary conditions to the electrode: the electrode conductivities are a function of the exchange current densities at the electrode boundary. The electronic potential at the electrode-electrolyte-interface was set to $\pm$135 mV for the respective electrode with the relative equilibrium potential of 0 mV. The boundary conditions for the electrolyte adjacent to the electrodes obey the Butler-Volmer equation for electrochemical reaction kinetics. We applied the diffusion coefficient D of 2.93 × 10−6 cm^2 s^{-1} in T = 298.15 K calculated by the Nernst-Einstein relation ($D = \mu RT/zF$) where μ is the ionic mobility, R the gas constant, T the absolute temperature, z the ionic charge, and F the Faraday's constant.

2.2.2. Fabrication of electronic conductivity gradient Li host (CG host)

Unitized electronic conductivity gradient host (CG host) were fabricated *via* a simple vacuum-assisted infiltration process.[42,43] A pristine cellulose nanofiber (CNF) suspension was obtained by repeated high pressure homogenization of pretreated wood cellulose powder (average size ~ 45 μm, KC Flock, Nippon Paper Chemicals) in IPA/water (=95/5, v/v) mixture solvent. The 5 wt.% (relative to the CNF weight) of colloidal SiO_2 nanoparticles (average particle size ~ 100 nm, Nissan) dispersed in water were then added into the CNF suspension. After vigorous mixing, the CNF@SiO_2 suspension was poured onto a PE (polyethylene) filter paper positioned inside a Porcelain Buchner funnel and then subjected to vacuum filtration. Then A 5 mg ml^{-1} concentration suspension of copper nanowires (CuNWs, average length = 20 μm, diameters 100 nm from Novarials Co. (USA)) in IPA with 0.5 wt.% hydrazine was blended with a CNF suspension, wherein the CuNW and CNF were controlled at ratio of 100:1, 30:1 and 10:1 (CuNW:CNF, wt:wt). And the CuNW@CNF mixture suspension was poured onto above-prepared CNF@SiO_2 layer, then CuNW suspension was introduced on top of the bi-layered host using the same infiltration method, resulting in wet-state tri-layered hetero-fibrous host. To facilitate the formation of a porous structure, the wet-state tri-layered hetero-fibrous host was conducted to freeze-drying, eventually producing a free-standing tri-layered hetero-fibrous host with highly developed pore structure.[43] The thickness of each layer in the hetero-fibrous host was controlled by

changing the amount of each suspension. The obtained hetero-fibrous host was then annealed under the H_2/Ar (5%/95%) flow at 230 °C for 3 h.

The theoretical calculation of the porosity of CG host was based on the assumption that the shape of the membrane is a well-defined cylinder. The volume of total cylinder shape was calculated through the multiplication of the bottom surface area and the thickness. The real volume occupied by the CuNW or CNF was obtained by dividing the mass of each layer by the density of CuNW or CNF. The subtraction of total cylinder shape by the real volume occupied by the Cu was the pore volume left in the membrane. The maximum amount of Li that can be accommodated in the membrane was the result of the total pore volume multiplied by the theoretical specific capacity density of Li (2062 mAh cm^{-3}).[44]

2.2.3. Structural/physicochemical characterization

The structure and physicochemical characteristics of the CG host were examined with field emission scanning electron microscopy (FE-SEM S-4800, Hitachi) in conjunction with energy-dispersive X-ray spectroscopy (EDS) and X-ray photoelectron spectroscopy (XPS K-alpha, Thermo Fisher) with monochromatized Al Kα radiation. The sp^2 C peak (284.5 eV) was used as the reference peak to calibrate other values. For the SEM observation of the lithiated host, batteries at Li plating/stripping process were first disassembled in the Ar-filled glove box to obtain the Li@host composites. The composites were then rinsed using DMC solvent to remove residual electrolyte and dried in the glove box for further SEM analysis. The electronic conductivities of each layer were measured using the four-point probe technique (CMT-SR1000N, Advanced Instrument Tech).

2.2.4. Electrochemical measurements

All of charge/discharge performances were measured using 2032-type coin cell with cycle testers (PNE Solution) at room temperature. Li||host and Li||Li@host cells were constructed using the Li metal foil of 200 μm thickness (Honjo Chemical Co.), Celgard 2320 separator, and 1M LiTFSI in DOL/DME (1:1, v:v) with 1 wt.% $LiNO_3$ additives as electrolyte (100 μl in each cell). For the Li||Li@host symmetric cells, 4 mAh cm^{-2} of Li was first deposited on each host at 2 mA cm^{-2} after pre-cycled host for 5 cycles to remove possible oxidation layer on the Cu at 50 μA. NCM811 ($LiNi_{0.8}Mn_{0.1}Co_{0.1}O_2$, LG Chemical Co.) active materials were used for full-cell assembly. The laminate of NCM811 electrode (~ 1.1 mAh cm^{-2}) was fabricated by casting NMP-based slurry mixture containing 90 wt.% of active material, 5 wt.% of carbon black and 5 wt.% of polyvinylidene fluoride binder on an aluminum current collector. After drying at 120 C, the electrodes were calendared and punched into disks with a diameter of 9 mm. The volume of the electrolyte (1M $LiPF_6$ in EC/DEC with 10 wt.% FEC, 1 wt.% VC additives) in the NCM811||Li@host full cells was 100 μl and Celgard 2320 separator was

used. The NCM811||Li@host full cells were tested between 3.0 and 4.2 V. All of the volumetric energy density was calculated with some assumption of using same thickness separator (20 μm), Al current collector (20 μm) and identical active area (diameters = 9 mm).

2.3. Results and discussion

2.3.1. Demonstration of electronic conductivity gradient effect

Figure 2.1 demonstrates conceptual illustration of Li plating behavior and Li-ion flux resulted from COMSOL Multiphysics for a theoretical examination on conventional Cu foil, Cu mesh (representative of conventional Li host) and the newly suggested CG host during Li plating. For Cu foil electrode, Li dendrite growth is accelerated due to the formation of 'hot-spot' resulted from a nonuniformity of initial Li nuclei or a cracked solid electrolyte interphase (SEI) during Li plating/stripping as shown in Figure 2.1a, it leads to consequent ramified Li filamentary growths and prompt consumption of the electrolyte with diminished Coulombic efficiency.[44-47] And the result of simulation can theoretically explain the formation of the 'hot-spot' on the Cu foil, the region of increased Li-ion flux is apparently visible in red color near the extruded nuclei and can facilitate dendritic growth and breakdown of SEI. A conventional Li host is known for its ability of improvement for cycle life in Li||Li symmetric cell by reducing a local current density, volume expansion due to its high electrochemical active area and the robust framework instead of host-less nature of lithium metal. However, because a conventional Li host also has high electronic conductivity in the thickness direction, show the focus of Li-ion flux on the top surface in red region, it means the issue of the Li dendritic growth on the top surface also occurs (Figure 2.1b).[38, 44] In contrast, the CG host has a unique structure with the increase of the electronic conductivity as it descends in the thickness direction. From this structural uniqueness, the significant concentration of Li-ion flux magnitude is suppressed on the top surface and show the color is blue as the proof of the weaken intensity of Li-ion flux in the simulation. On the other hand, the red color region which means the intense Li-ion flux form on the inner space of the bottom layer with high electronic conductivity. Eventually, The Li plating is concentrated on the highly electronic conductive bottom layer and the the Li dendritic growth on the top surface without the electron conduction ability is significantly suppressed as shown in the scheme. In addition, the middle layer with well-tailored electronic conductivity can provide the wasted dead Li particles with facile electron and ion transfer and utilize their capacities to a higher extent (Figure 2.1c).[38]

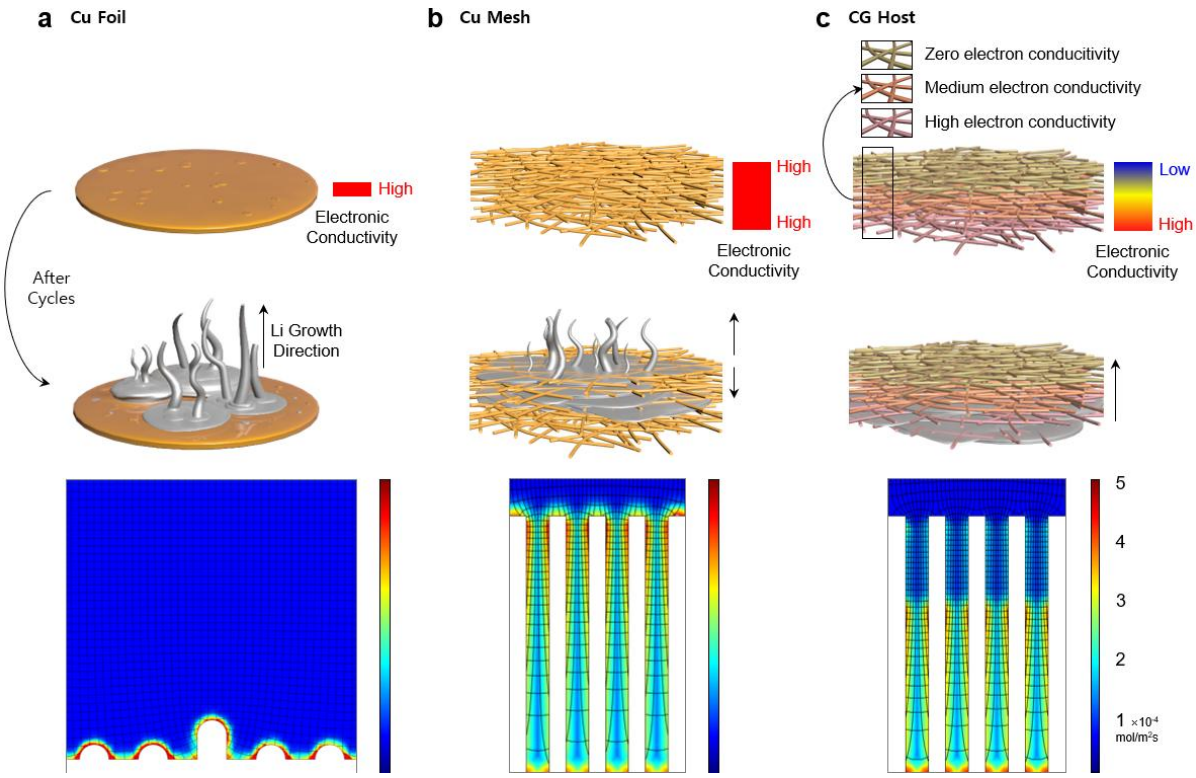

Figure 2.1. Conceptual illustration and COMSOL Multiphysics of Li plating on (a) Cu foil, (b) Cu mesh and (c) CG host.

2.3.2. Characterization of electronic conductivity gradient Li host (CG host)

Hetero-fibrous CG host was fabricated through a simple vacuum-assisted infiltration process analogous to a traditional paper-making method.[42,43] A CNF suspension (in a mixed solvent of isopropyl alcohol (IPA)/water (=95/5 (v/v))) blended with the SiO_2 nanoparticle suspension as CNF disassembled agent for well-developed porous CNF layer was prepared and poured onto PE (polyethylene) filter paper to fabricate a porous CNF@SiO_2 layer. A CuNW suspension mixed with a CNF suspension was subsequently poured onto the above-prepared CNF@SiO_2 layer. A CuNW suspension was then introduced on top of the CuNW@CNF layer of the bi-layered structure using the same infiltration method, resulting in a hetero-fibrous tri-layered CG host. After undergoing freeze-drying, which is known to effectively suppress dense packing of CNFs,[43] annealing process for CuNW activation, a free-standing tri-layered hetero-fibrous CG host with well-developed pore and electronic conductivity gradient structure was acquired (Figure 2.2a). The obtained CG host showed a mechanically robust property through the bending state of CG host inset image. Cross-sectional scanning electron microscopy (SEM) image (Figure 2.2b) showed that CuNW layer (bottom layer, 30 μm), CuNW@CNF layer (middle layer, 14 μm) and CNF@SiO_2 layer (top layer, 1 μm) were well integrated. Comparison of C/Cu content ratio for each layer thorough EDX spectrum analysis demonstrated that CNF content decrease as it descends in thickness direction into bottom layer explained realization of a well-defined gradient structure (Figure 2.3). In final, the unitized hetero-fibrous CG host can accommodate 7.02 mAh cm^{-2} of maximum Li capacity when we calculate the theoretical loading of Li metal according to the void space volume in the CG host, showing that the CG host is the ideal robust 3D Li host for high energy density Li metal battery (Table 2.1).

Prior to electronic characterization of CG host, because the electronic conductivity of CuNW membrane considerably depends on an annealing process, we conducted the X-ray photoelectron spectroscopy (XPS) of CuNW membrane to analyze effect of thermal annealing for CuNW membrane (Figure 2.4a). In the case of as-prepared CuNW membrane, the existence of a peak at 933.9 eV and 934.9 eV attributed to CuO and $Cu(OH)_2$ respectively is the evidence of the oxidized surface which results in the high electronic resistance of the CuNW network (Figure 2.4b). In contrast, the XPS analysis of CuNW membrane undergoing thermal annealing under the H_2/Ar (5%/95%) at 230 ^oC for 3 h confirmed the reduction on the oxidized surface of CuNW, and the acquired CuNW membrane showed high electronic conductivity due to well-connected CuNW network (Figure 2.4c).[44,48]

As shown in Figure 2.2c, the formation of highly connected electron conducting network in CuNW layer (bottom layer) is clearly visible in the surface morphology due to reduced surface of CuNW building block via thermal annealing and it leads to low electronic resistance (0.1 Ω) of CuNW layer. On the other hand, surface morphology of CuNW@CNF layer (middle layer) shows that CuNW is intermingled with an electronically inert CNF, because of this structural character, the electronic

resistance of CuNW@CNF layer is 0.9 Ω. It means the middle layer can conduct electrons but has lower electronic conductivity than it of bottom layer. CNF@SiO_2 layer (top layer) which is composed of electronic insulators is electronically non-conductive as we expect, and the surface morphology of it (Figure 2.2e) delivers well-develop porous CNF layer with fully dispersed SiO_2 nanoparticles. Additionally, polar groups in CNF and SiO_2 nanoparticles support that CG host has superior wettability of electrolyte.[40]

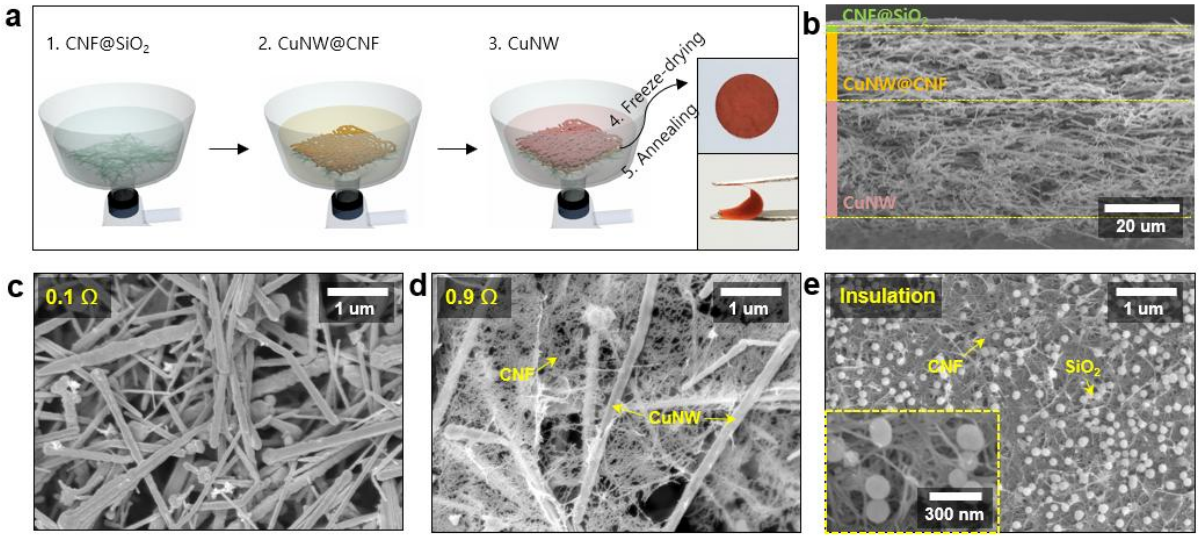

Figure 2.2. Fabrication and characteristics of CG host. (a) Schematic representation and photographs (insets) demonstrating the fabrication and the structural robustness of CG host. (b) SEM image for the cross-section view of CG host. SEM image of the surface view for each layer (c) bottom layer (CuNW) (d) middle layer (CuNW@CNF) (e) top layer (CNF@SiO_2).

	Weight (mg)	Bottom surface area (cm^2)	Thickness (μm)	Porosity (%)	Electric conductivity ($S\ cm^{-1}$)	Maximum Li Capacity ($mAh\ cm^{-2}$)
Top layer (CNF@SiO2)	0.05	0.785	1	54.504	-	-
Middle layer (CuNW@CNF)	2.62	0.785	14	68.545	1880	1.979
Bottom layer (CuNW)	3.87	0.785	30	81.504	7840	5.041

Table 2.1. Textural parameters of each layer in the electronic conductivity gradient host (CG Host).

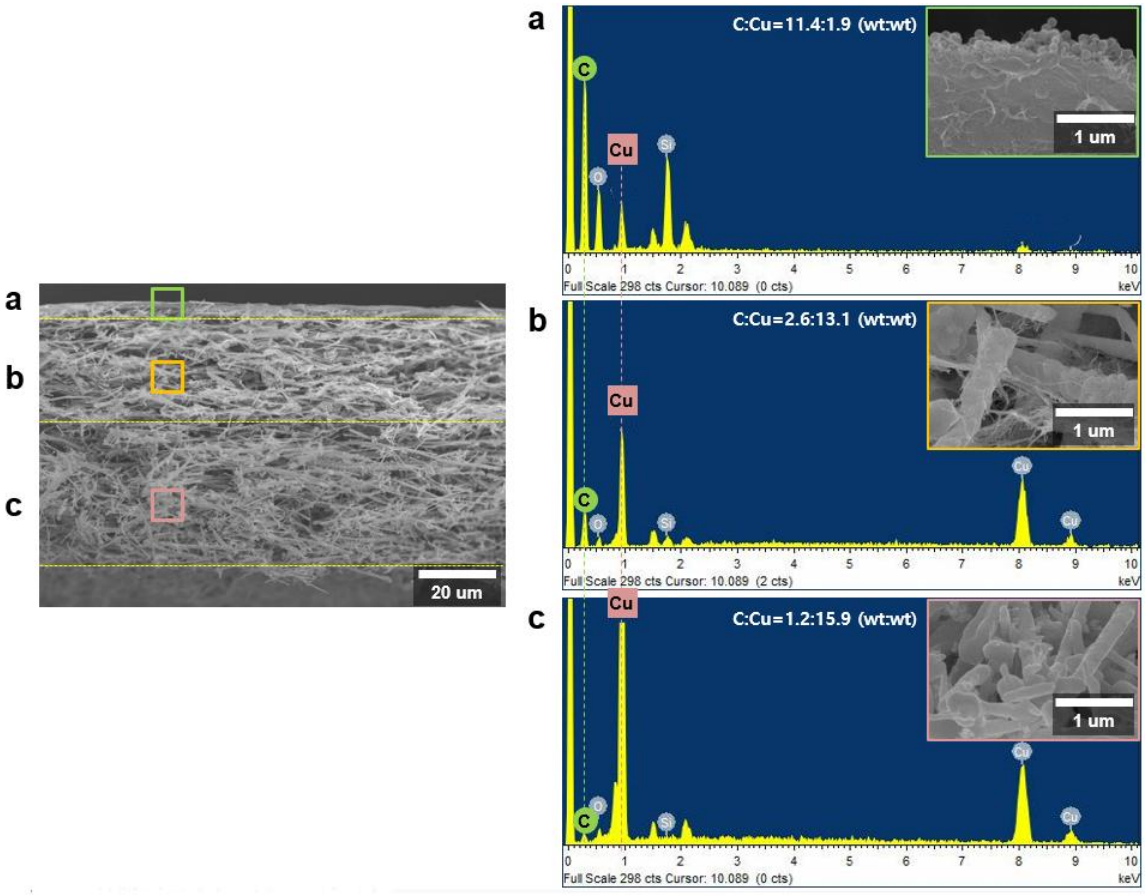

Figure 2.3. Characterization of the electronic conductivity gradient host via elemental EDX spectrum. Morphology of each layer highlighted with different colors in the cross-section SEM image of CG host. The inset SEM images and corresponding elemental EDX spectrum of (a) top layer (CNF@SiO_2), (b) middle layer (CuNW@CNF) and (c) bottom layer (CuNW)

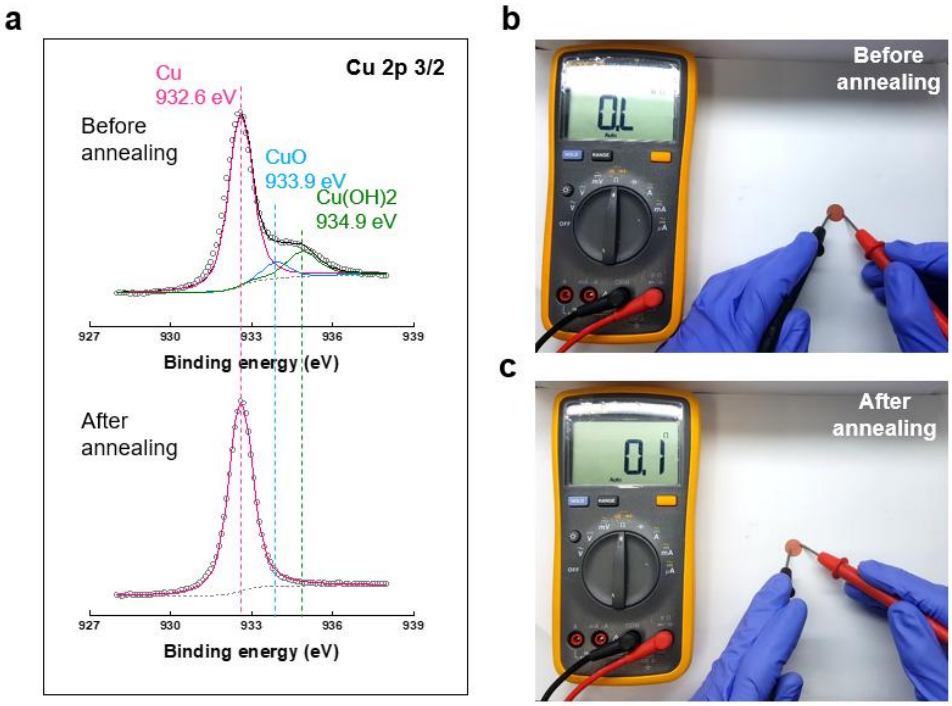

Figure 2.4. Electronic characterization of the CuNW before and after annealing. (a) XPS spectrum of the CuNW before and after annealing. Photographs of the multi-meter measurement for CuNW (b) before and (c) after annealing process.

2.3.3. Effect for Li protection and plating/stripping behavior

To clearly investigate the spatial distribution of Li plating/stripping of CG host, we characterized the cross-section of the CG host at different depth of charge (DOC) of Li plating/stripping by SEM (Figure 2.5a). We assume that the DOC of pristine CG host before Li plating is 0% (Figure 2.5b) and the DOC after Li plating as theoretical maximum Li capacity is 100%. When plating 3 mAh cm^{-2} (DOC 42%, Figure 2.5c) Li on the CG host, densely deposited Li is observed on bottom layer due to its high electronic conductivity. Upon increasing the Li plating areal capacity to 7 mAh cm^{-2} (DOC 100%, Figure 2.5d), the cross-sectional image shows that plated Li entirely fell up all the pore volume in the CG host except for the top layer. When the deposited Li was gradually stripped from the CG host electrode with 2 mAh cm^{-2} (DOC 71%, Figure 2.5e), Li stripping occurred on the top surface of plated Li during the previously Li plating process because the previous plated Li acted as major electron conductor instead of CG host. In Final, the CG host remained its initial morphology after a complete Li stripping (DOC 0%, Figure 2.5f). All the deposited Li metal was reversibly stripped from CG host with the intact 3D structure, proving its mechanically robust characteristic.

To investigate the role of CG host with different thickness of top layer in Li plating/stripping behavior and suppressing dendrites, galvanostatic cycling measurements were conducted with Li||Li@CG Host cell symmetric cell and SEM images and photographs of appearance after 20 plating/stripping cycles are shown in Figure 2.7. In case of Cu foil (Figure 2.6a), the optical image of Cu foil after cycles showed unevenly deposited Li and a developed Li dendrite, dead Li was easily detected due to unstable Li/electrolyte interface during Li plating/stripping process. And surface morphology of CG host without top layer (T=0 μm) (Figure 2.6b) showed an extruded Li metal grown from bottom layer due to its electronic conductivity gradient structure, however, the appearance in the inset of photo displayed exposure Li deposits on the top surface. In contrast, the photographs of CG host with a top layer (T=1, 10 μm) show a pink and grey color surface which are attributed from pre-deposited Li and CuNW inside the host and the surface morphology of top layer shows that the Li nucleation on the top surface is effectively blocked after even 20 cycles (Figure 2.6c, d). It proves that the existence of top layer works to prevent Li nucleation of top surface and support formation of Li-ion flux. As illustrated in Figure 2.7a, the symmetric cell with Cu foil current collector as anode exhibited an abrupt rise in the stripping voltage from the Cu foil over 70 h. It addresses consumption of pre-deposited Li on Cu foil because dendritic Li continuously grows during Li plating/stripping process. On the other hand, CG host with thick top layer (T=10 μm) showed occurrence of increase for stripping voltage after 35 h, while for CG host without top layer (T=0 μm), the cell displayed 110 h of cyclability. In contrast, the cyclability of CG host with thin top layer (T=1 μm) obviously increased over 220 h and it is far superior value to that of different thickness CG hosts (T=0, 10 μm).

A gradual rise in Li plating/stripping overpotential in the voltage profile is also observed with the increase in thickness of its top layer resulting in a rise of tortuosity for Li-ion path (inset). This influence can explain the lower cyclability of the CG host with thick top layer (T=10 μm) than that of Cu foil. CG host without top layer (T=0 μm) can deliver slightly better cycle life than the value of Cu foil due to its 3D electronic conductivity gradient architecture, however, the Li deposits grown from bottom layer still can be observed on the top surface due to lack of non-conductive top layer and it leads to appearance of dead Li same in case of Cu foil. Conversely, the great improvement of cycling stability in CG host with thin top layer (T=1 μm) can be attribute to the structural uniqueness and proper thickness of top layer which support suppression of top surface Li growth and formation of uniform Li-ion flux. Figure 2.7b demonstrates results of COMSOL Multiphysics according to thickness of top layer to further verify the aforementioned effects by thickness of top layer. Results of CG host with and without top layer (T=0, 1 μm) are seen to be similar behavior in Li-ion flux to focus into the bottom of electrode geometry. However, on the top surface of the CG host without top layer, slightly brighter blue color which indicates higher concentration of Li-ion flux than the value of CG host with top layer is shown, demonstrating that the Li nucleation could be occur on top surface. On the other side, when the thick top layer is introduced into the electrode geometry, the ionic flux within the columnar pores displays significantly lower concentration than values of the other CG host. This phenomenon in the simulation is in good agreement with the high overpotential on CG host with thick top layer during Li plating/stripping.

Apart from thickness of top layer, an electronic conductive ability of middle layer can also vary Li plating/stripping behavior. Therefore, LI plating/stripping galvanostatic cycling test was carried out with a difference ($\Delta\sigma$=7.5, 6 and 4 kS cm^{-1}) between a fixed electronic conductivity of bottom layer and variable that of middle layer, respectively (Figure 2.7c). The ability for conducting electrons in the middle layer can be controlled by adjusting the composition of electronic conducting building block (CuNW) and electronic insulating building block (CNF) and it was proved by four-point probe method (Table 2.2). As shown in Figure 2.7c, the symmetric cell of CG host with the lowest difference ($\Delta\sigma$=4 kS cm^{-1}) of electronic conductivity retained the stable voltage profile of Li plating/stripping until 160 h, while for the CG host with the highest difference ($\Delta\sigma$=7.5 kS cm^{-1}) of the conductivity, the cycle life showed only 60 h. And the medium value ($\Delta\sigma$=6 kS cm^{-1}) in the differences of the electronic conductivity indicated the excellent cycle durability over 220 h. the simulation was also conducted to theoretically verify the cyclability depended on the different value between electronic conductivity of bottom and middle layer (Figure 2.7d). When the CG host has the lowest difference of the conductivity ($\Delta\sigma$=4 kS cm^{-1}), the result shows a red spot, which means the concentrated Li-ion flux, on the middle layer because of its relatively high electron conductivity, indicating that the Li nucleation could occur on the spot. This Li nucleation on the spot of middle layer could also develop to dead Li, resulting in

the low cyclability. For the highest value of difference of the conductivities ($\Delta\ \sigma$=7.5 kS cm^{-1}), significantly low Li-ion flux within the middle layer with comparably low electronic conductivity is clearly visible. This phenomenon means the middle layer of low conductivity could act as thick non-conductive layer cause blocking Li-ion path and the poor ability of capturing dead Li, demonstrating the low cycle life. In contrast, the middle layer with the well-tailored electronic conductivity ($\Delta\ \sigma$=6 kS cm^{-1}) can help to guide uniform Li-ion flux into the bottom layer and capture dead Li generated from bottom layer. These advantages can explain the superb cycle span of the above Li plating/stripping result.

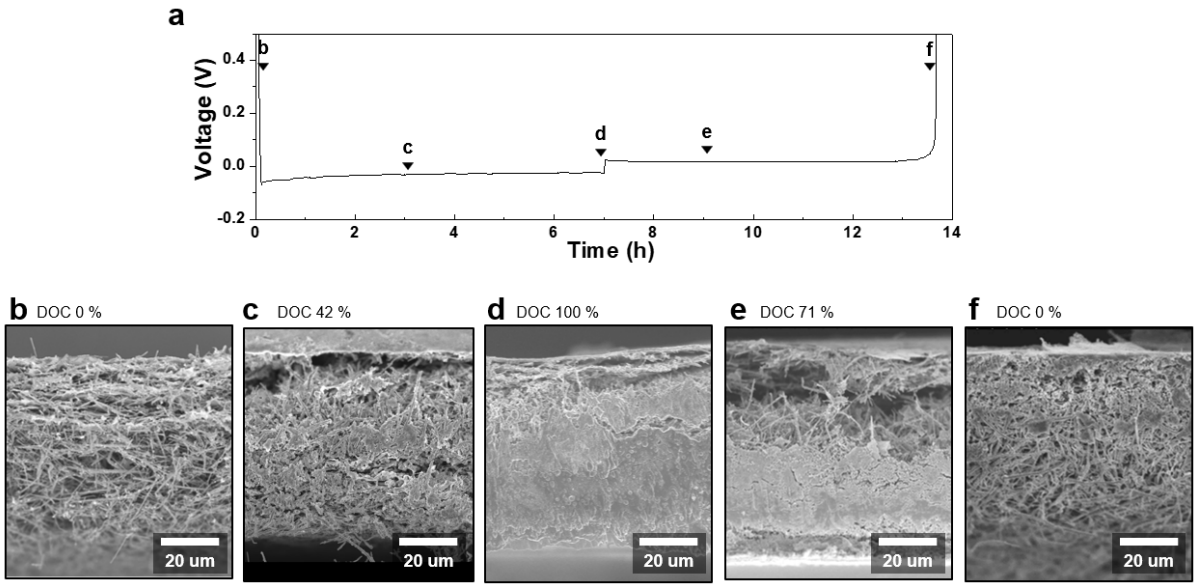

Figure 2.5. The Li plating/stripping behavior on/from the CG host in detail via SEM images. (a) Li plating/stripping states in the galvanostatic discharge/charge voltage profile at 1 mA cm^{-2}. The cross-section view SEM images of (b) the pristine CG host (DOC 0%) and after Li plating (c) 3 mAh cm^{-2} (DOC 42%) (d) 7 mAh cm^{-2} (DOC 100%). SEM images of CG host after stripping (e) 2 mAh cm^{-2} (DOC 71%), (f) 7 mAh cm^{-2} (DOC 0%).

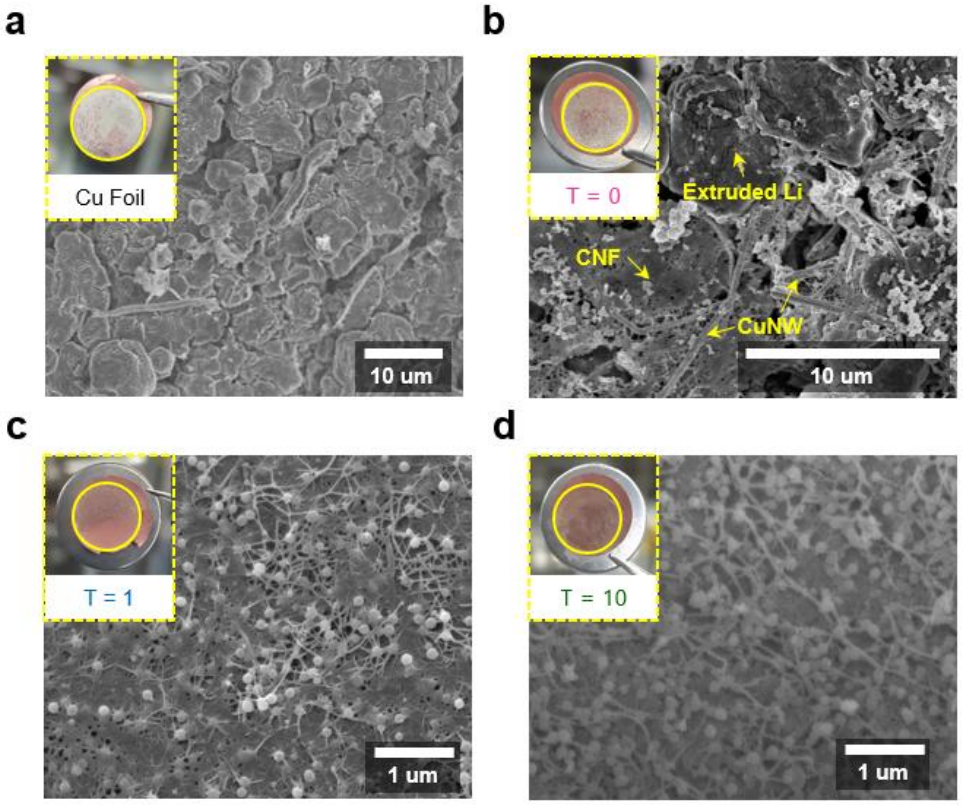

Figure 2.6. Surface morphology and photographs after 20 cycles of Li plating/stripping at 0.5 mA cm^{-2} on (a) Cu foil and CG host (b) without and (c) with thin (1 μm) and (d) thick (10 μm) top layer (CNF@SiO_2).

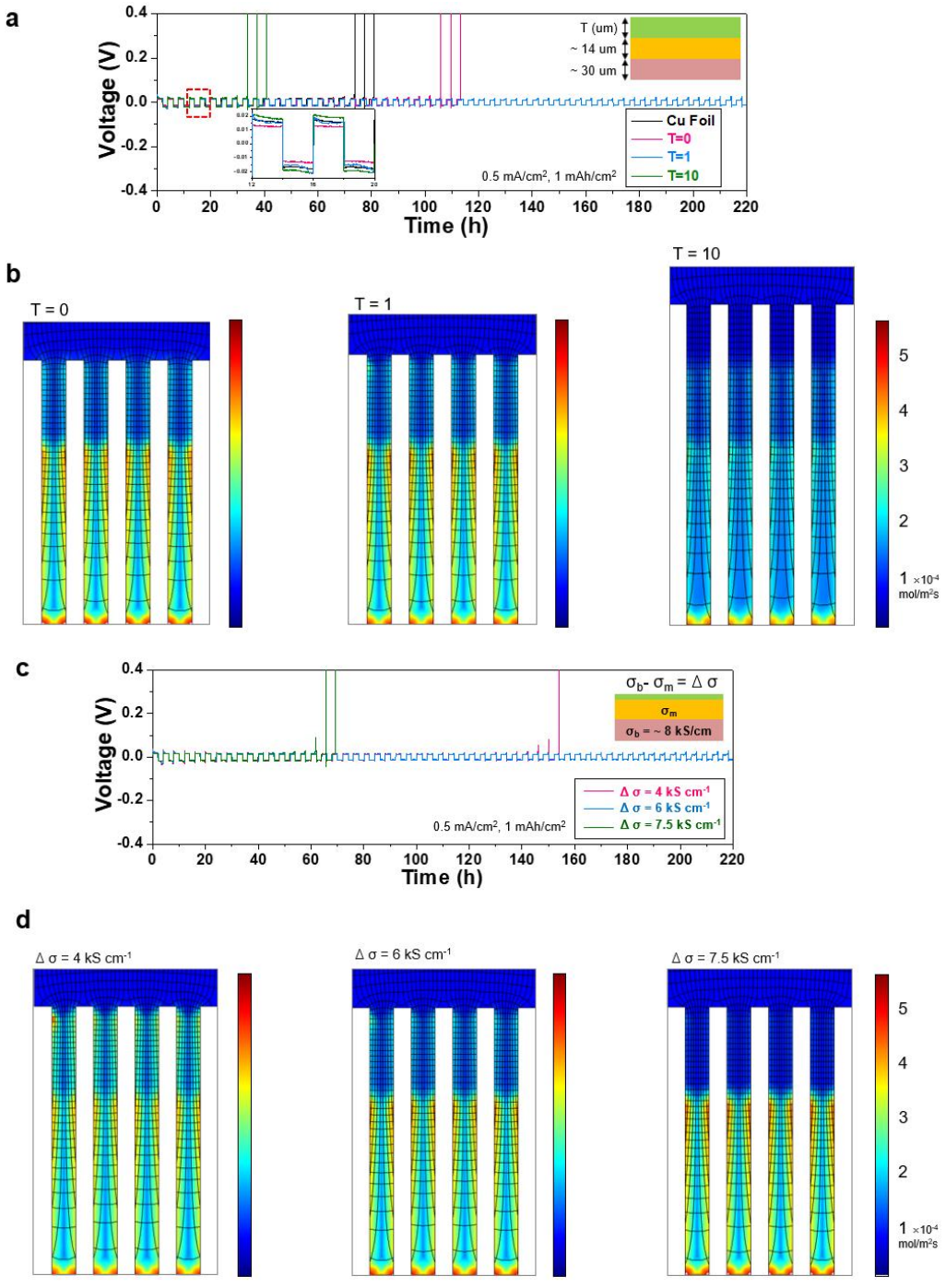

Figure 2.7. Optimization of CG host structure for stable Li plating/stripping. (a) and (b) Thickness of top layer (CNF@SiO_2). (c) and (d) Electronic conductivity difference between middle (CuNW@CNF) and bottom layer (CuNW).

CuNW:CNF (wt:wt)	**100:0**	**100:1**	**30:1**	**10:1**
Electric Conductivity ($S\ cm^{-1}$)	7840	3760	1880	460
Sheet Resistance (four-point probe, mΩ/sq)	35	100	307	544
Bulk Resistance (Multimeter, mΩ)	100	400	900	1200

Table 2.2. Electronic parameters of middle (CuNW@CNF) layer depending on different composition of CuNW and CNF.

2.3.4. Electrochemical performance of CG Host

To better understand the ability of CG host in prevention of Li dendrite, galvanostatic cycling measurements were conducted with symmetrical cells. The cells were cycled with a capacity of 1 mAh cm^{-2} at a function of current density. As shown in Figure 2.8a, Cu foil used as the current collector for the anodes indicated a gradual increase in voltage hysteresis after 10 cycles, and the soaring overpotential was observed over 25 cycles at 1 mA cm^{-2} of current density. Additionally, CuNW membrane, which is representative of conventional 3D Li host known as suppressing Li dendrite due to its 3D porous structure, showed relatively low voltage hysteresis (~ 40 mV) and better cycling stability than it of Cu foil. However, after 35 cycles, the voltage oscillation in Li plating/stripping was visible and then the cycle life cannot reach over 50 cycles. While for CG host, the cell revealed a stabilized low voltage hysteresis (~ 22 mV) in a few cycles and a great improvement in cycling stability even over 250 cycles. These results display that the CG host presents the Li dendrite growth has been alleviated, which results in a stable SEI layer by the structural uniqueness. This performance of CG host in cycling stability is outstanding between the CG host and other metallic Li hosts in the reported results shown in Table 2.3, to the best of our knowledge.

Coulombic efficiency, defined as the ratio of Li stripping capacity to plating capacity, is another important factor to value the electrochemical performance of Li metal anode, demonstrating the reversibility during Li plating/stripping process. The Coulombic efficiency was tested with plating 1 mA cm^{-2} capacity of Li at 0.5 mA cm^{-2} of current density and then stripping the deposited Li up to 0.5 V (vs Li^+/Li) as summarized in Figure 2.8b. The CG host sample presented stable Li plating/stripping behavior (Figure 2.9b) and the high Coulombic efficiency with a retention above 96% for more than 120 cycles. The cell with Cu foil maintained also Coulombic efficiency above 96% for 80 cycles, then decreased gradually up to ~60% in the following cycles and the value of Coulombic efficiency start to randomly oscillate after 100 cycles, the inferior value of coulombic efficiency retention of Cu foil was ascribed from the uneven Li-ion flux and Li dendrite growth, corresponding to previous reports.[25,26,46] Meanwhile, benefitting from the structural uniqueness, which cause reduced local current density, suppression of dead Li and Li dendrite growth on top surface, the CG host displayed improved Coulombic efficiency retention.

For verifying the galvanostatic cycling performance, electrochemical impedance spectroscopy (EIS) for as-assembled symmetric cell was carried out. (Figure 2.10) The cell with CG host showed consistent decrease of SEI resistance (R_{int}) and charge transfer resistance (R_{ct}) from 1st cycle to 50th cycle attributed from 3D network and stable SEI formation (Figure 2.10c), [48-51] resulting in excellent cycling performance. Otherwise, Cu foil displayed a rise in both of resistance after 30th cycle and it mean that the Li deposits was continuously consumed by reacting with electrolyte, accelerating forming thick SEI which cause increasing interfacial resistance (Figure 2.10b).

The CG host was used for more in-depth understanding in which the anode was paired with a NCM811 cathode to fabricate Li metal battery full-cell. The N/P ratio, which balance the capacity ratio between anode and cathode in the cell, was controlled about 3.6, meaning that the capacity of Li in the anode has 3.6 times than that of the cathode. The NCM811 cathode is already lithiated, the N/P ratio can be interpreted as an excess Li capacity in the anode for Li metal battery. We explored the feasibility of the CG host in Li metal battery system and first reported the Li host assembled with a NCM811 cathode in the previous Li host studies.

The results reported in Figure 2.8c display that cells composed of the Li@CG host anode and NCM811 cathode operated under 1 C. Cells were first cycled at a low rate 0.1 C (calculated based on the NCM811 cathode) for the initial three cycles to form a stable SEI and then 1 C for the subsequent cycles. The CG host delivered superior capacity retention (~90%) and extremely high Coulombic efficiency (99.8%) over 100 cycles. Meanwhile, the cell assembled with Li@Cu foil indicated gradual capacity decay from 20th cycle and then reached a capacity retention of 37.6% after 80 cycles. This degradation of the cell using the Cu foil as current collector is originated from continuous Li consumption and Li dendrite growth by reaction between electrolyte and Li deposits during charge and discharge state.[25,45,48,49] In contrast, CG host showed stable operation of the Li metal battery full-cell by alleviating the Li dendrite growth on top surface and dead Li ascribed to its structural advantages of electronic conductivity gradient. With these structural characteristics, CG host has higher value of volumetric energy density in the previously reported Li host studies and proves that the electronic conductivity gradient structure is a rational architecture of Li host for high energy density Li metal battery (Table 2.4). The volumetric energy density was calculated a specific capacity at 0.1 C divided by a sum of volume for separator, current collector, active material in cathode and a lithiated Li host.[50]

For detailed demonstration of cycling performance, the voltage profile is shown in Figure 2.11. The CG host revealed stable voltage profile without huge change of the profile over 50 cycles and the charge/discharge intersection point from the curved slightly moved horizontally leftward, indicating stable electrochemical performance of CG host anode in Li metal battery full-cell. To examine the mechanism for the superior electrochemical performance of CG host, morphology study after 100 cycles of NCM811||Li@host full-cell is shown in Figure 2.8d. The surface morphology of CG host shows an intact top layer composed of CNF and SiO_2 nanoparticles and no Li dendrite growth on the top surface even after 100 cycles, the result contrasts with the surface morphology of Cu foil which the developed Li dendrite and isolated dead Li is easily observed (Figure 2.12). These evidences can demonstrate the improved cycling stability of CG host.

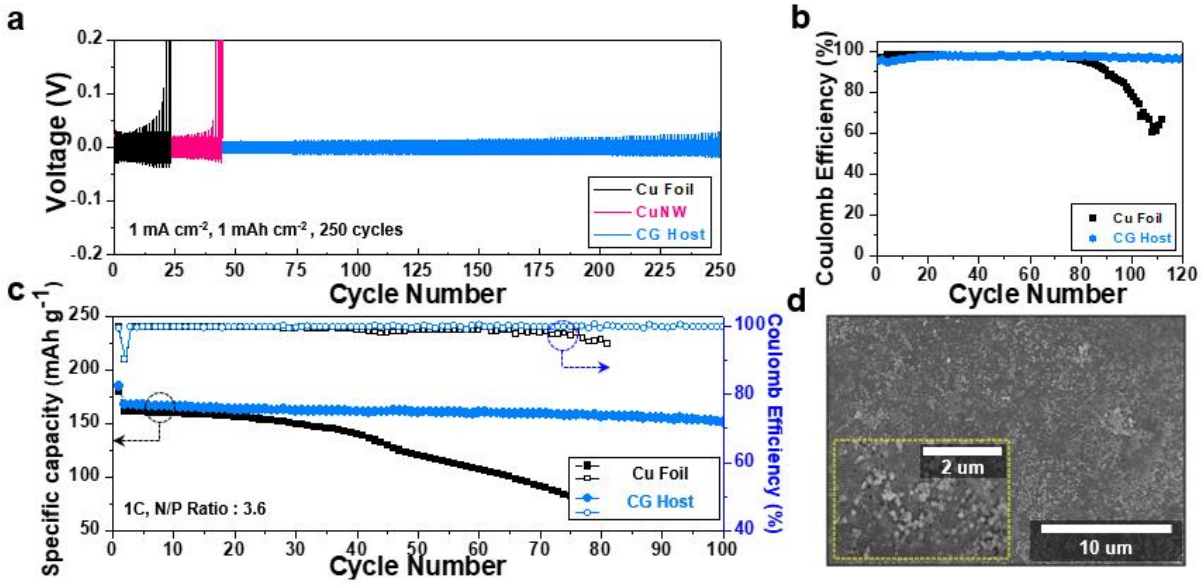

Figure 2.8. Electrochemical performance in cells with different Li host. (a) Galvanostatic Li plating/stripping voltage profile for the Li||Li@host symmetric cell using Cu foil, CuNW and CG host at 1 mA cm^{-2} for 1 mAh cm^{-2} and (b) Comparison of the Coulombic efficiency for Li||host asymmetric cell using Cu foil, CuNW and CG host at 0.5 mA cm^{-2} for 1 mAh cm^{-2}. (c) Cycling performance of the NCM811 full-cell using Cu foil and CG host at 1 C (d) Surface morphology on CG host after 100 cycles of NCM811||Li@host full-cell

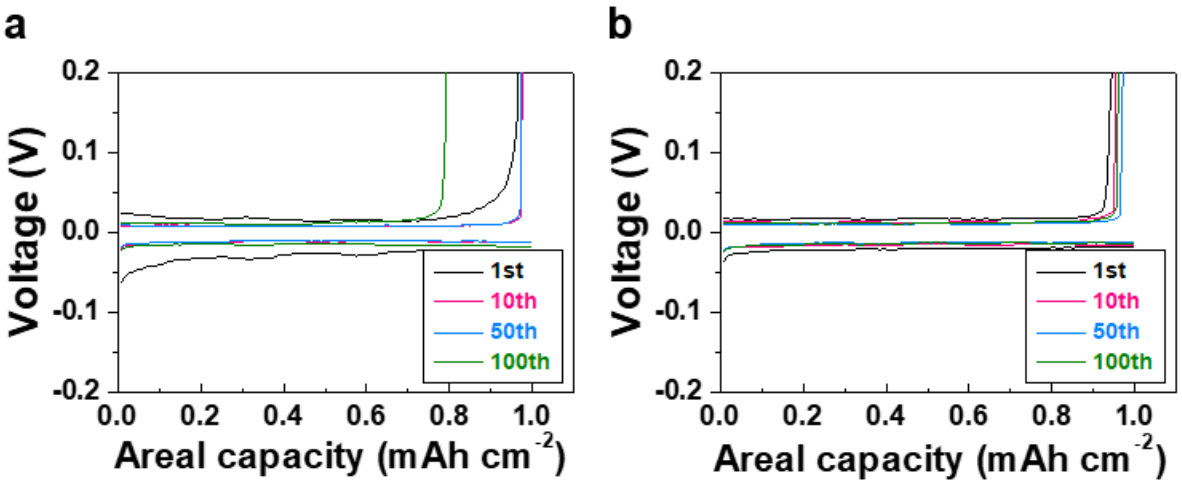

Figure 2.9. Voltage profiles of Li plating/stripping on (a) Cu foil and (b) CG host with current density of 1 mA cm^{-2} for 1 mAh cm^{-2}.

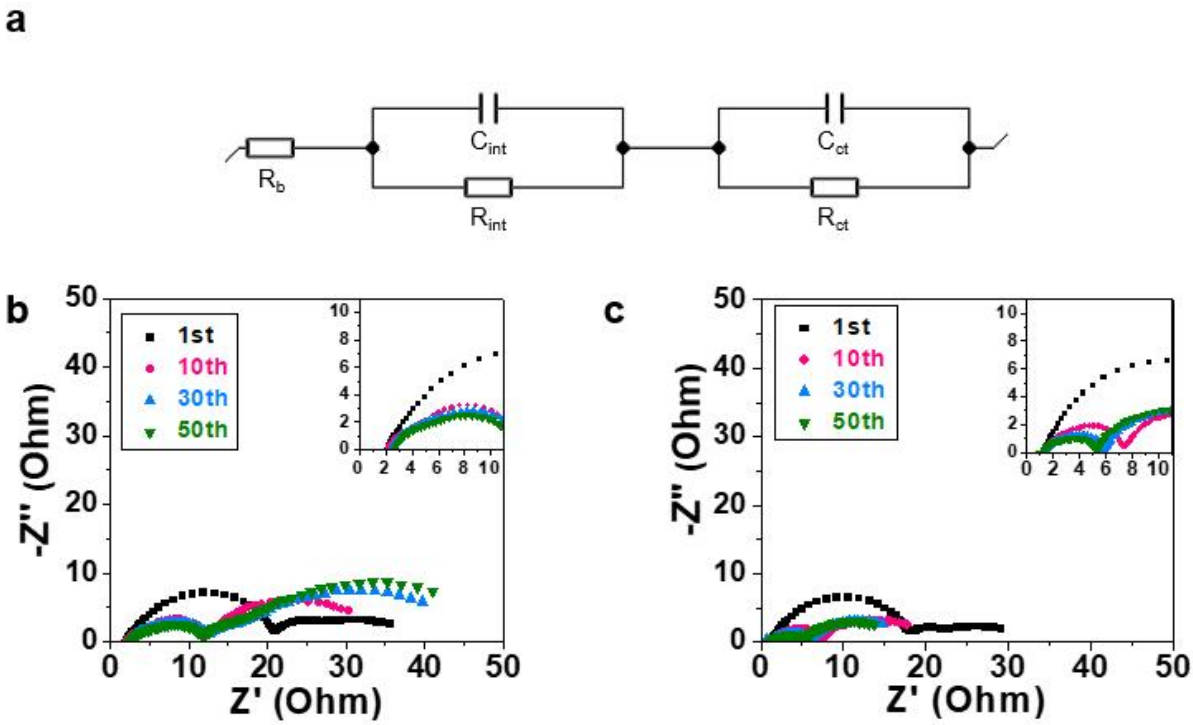

Figure 2.10. Impedance spectra study of the CG host electrode for Li plating/stripping at 1 mA cm^{-2}. (a) The corresponding equivalent circuit model. Impedance spectra for the cell using (b) Cu foil and (c) CG host

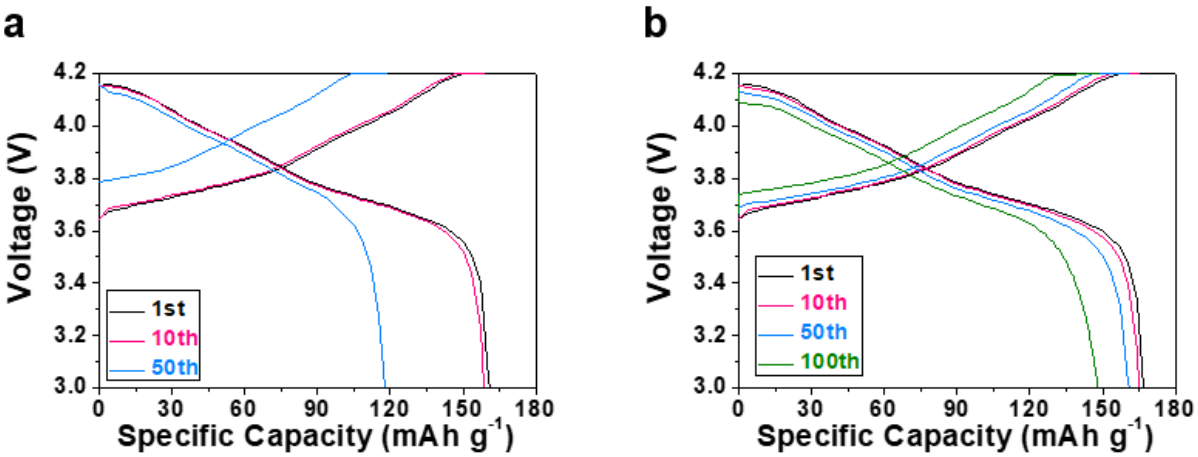

Figure 2.11. Voltage profiles for NCM811||Li@host for (a) Cu foil and (b) CG host under 1C.

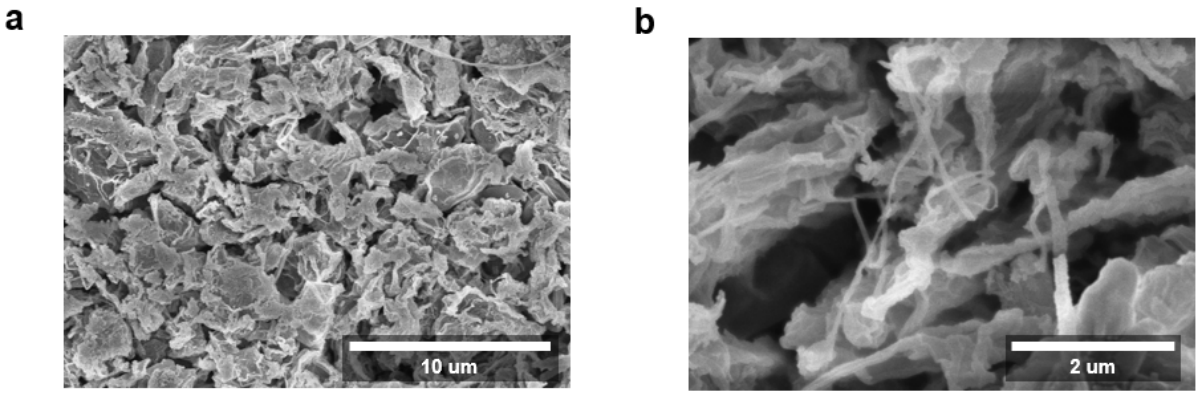

Figure 2.12. Surface morphology of Cu foil after 100 cycles of NCM811||Li@host full-cell.

Li host Thickness (μm)	Operation capacity (mAh cm^{-2})	Current density (mA cm^{-2})	Li/Li symmetric cell Cycles	Ref
45	**1**	**1**	**250**	**This work**
-	0.5	0.2	120	44
20	0.5	0.2	200	45
52	2	1	110	43
70	1	1	100	24
45	0.5	0.2	100	35
200	0.5	0.5	250	25
-	1	0.5	125	51
20	0.5	0.5	200	52

Table 2.3. Parameters for cycling performance of previously reported papers about metallic Li host for Li metal batteries.

Li host thickness (μm)	Active material	Active material loading level (mAh cm^{-2})	N/P ratio	C-rate	Volumetric energy density (Wh L^{-1})	Ref
45	**NCM811**	**1.10**	**3.6**	**1 C**	**359**	**This work**
20	LFP	0.3	6.7	0.5 C	187	45
52	LCO	0.17	14.7	5 C	-	43
70	LFP	1	3	0.5 C	266	24
200	LFP	0.34	Molten Li	2 C	67	26
1000	LFP	2	4	0.5 C	-	48
115	LFP	2.21	2.7	0.5 C	216	53

Table 2.4. Summary of representative papers previously reported papers about Li host for Li metal battery full cell.

2.4. Conclusion

In summary, we have presented electronic conductivity gradient Li host (CG host) based on hetero-fibrous scaffold composed of highly conductive 1D building blocks (Copper nanowire, CuNW) and electronic insulated 1D building blocks (Cellulose nanofiber, CNF) with mechanical flexibility, resulting in uniform Li deposition inside the hetero-fibrous CG host and highly stable cycling performance. The results of COMSOL Multiphysics revealed that electronic conductivity gradient structure effectively offered Li deposition into inner space due to its structural peculiarity compared with using the planar Cu, conventional 3D Li host with the high electronic conductivity in the thickness direction. The effects of thickness of top layer and difference between conductivity of bottom layer and middle layer were also confirmed based on the simulation and galvanostatic cycling test. Moreover, the Li plating/stripping behavior and structure stability of CG host showed excellent reversibility after even Li plating/stripping for 7 mAh cm^{-2}. In addition to the theoretically proved structural uniqueness from the simulation, the evenly distributed Li-ion flux by the polar group of CNF and dead Li capturing ability of middle layer with well-tailored conductivity supported to achieve substantial improvements in the cycling stability and high coulombic efficiency in symmetric cell configuration. Furthermore, to the best of our knowledge, CG host also offers higher energy density full-cell assembled with NCM811 cathode compared to previous other Li host studies due to these featured structural characteristics of electronic conductivity gradient structure. We believe that our new rational structure of Li host shows new directions to realize reversible Li plating/stripping behaviors and contribute to the practical development of high energy density lithium metal batteries.

III. References

1. P. Arora, Z. Zhang, *Chem. Rev*. **2004**, 104, 4419
2. M. Yoshio, R. J. Brodd, A. Kozawa, *Lithium-Ion Batteries*, **2009**, *49-51*
3. S. Goriparti, E. Miele, F. D. Angelis, E. D. Fabrizio, R. P. Zaccaria and C. Capiglia, *J. Power Sources.*, **2014**, *257*, 421-443
4. S. K. Marka and V. V.S.S. Srikanth, *Nanosci. Nanotechnol-Asia*, **2015**, 5, 90-108
5. J. B. Goodenough and K.-S. Park, *J. Am. Chem. Soc.,* **2013**, 135, 4, 1167-1176
6. C. Liu, Z. G. Neale and G. Cao, *Mater. Today*, **2016**, 2, 19, 109-123
7. C. K. Chan, X. F. Zhang and Y. Cui, *Nano Lett.*, **2008**, 8, 1
8. G. Derrien, J. Hassoun, S. Panero, and B. Scrosati, *Adv. Mater.,* **2007**, 19, 2336–2340
9. L. Li, Z. Wu, S. Yuan and X.-B. Zhang, *Energy Environ. Sci.*, **2014**, 7, 2101
10. H.-J. Peng, J.-Q. Huang and Q. Zhang, *Chem. Soc. Rev.*, **2017**, 46, 5237
11. D. Lin, Y. Liu and Y. Cui, *Nat. Nanotech*., **2017**, 12, 194
12. B. L, J.-G. Zhang and W. Xu, *Joule*, **2018**, 2, 1-13
13. J.-M. Tarascon and M. Armand, *Nature*, **2001**, 414, 369
14. W. Xu, J. Wang, F. Ding, X. Chen, E. Nasybulin, Y. Zhangad and J.-G. Zhang, *Energy Environ. Sci.*, **2014**, 7, 513
15. X.-B. Cheng, R. Zhang, C.-Z. Zhao and Q. Zhang, *Chem. Rev.*, **2017**, D-E
16. J. Qian, W. A. Henderson, W. Xu, P. Bhattacharya, M. Engelhard, O. Borodin and J.-G. Zhang, *Nat. Commun.*, **2015**, *6*, 6362
17. W. Li, H. Yao, K. Yan, G. Zheng, Z. Liang, Y.-M. Chiang and Y. Cui, *Nat. Commun.*, **2015**, *6*, 7436-7443
18. D.-J. Yoo, K. J. Kim and J. W. Choi, *Adv. Energy Mater.*, **2018**, 1702744
19. S. Jurng, Z. L. Brown, J. Kim and B. L. Lucht, *Energy Environ. Sci.*, **2018**, 11, 2600-2608
20. G. Zheng, S. W. Lee, Z. Liang, H.-W. Lee, K. Yan, H. Yao, H. Wang, W. Li, S. Chu and Y. Cui, *Nat. Nanotech*., **2014**, *9*, 618-623
21. J. Xie, L. Liao, Y. Gong, Y. Li, F. Shi, A. Pei, J. Sun, R. Zhang, B. Kong, R. Subbaraman, J. Christensen and Y. Cui, *Sci. Adv*. **2017**, 3, 3170

22. H. Zhang, X. Liao, Y. Guan, Y. Xiang, M. Li, W. Zhang, X. Zhu, H. Ming, L. Lu, J. Qiu, Y. Huang, G. Cao, Y. Yang, L. Mai, Y. Zhao and H. Zhang, *Nat. Commun.*, **2018**, 9, 3729

23. M. S. Kim, J.-H. Ryu, Deepika, Y. R. Lim, I. W. Nah, K.-R. Lee, L. A. Archer and W. I. Cho, *Nat. Energy,* 2018, 3, 889–898

24. W. Liu, D. Lin, A. Pei and Y. Cui, *J. Am. Chem. Soc.,* **2016**, 138, 15443−15450

25. S.-H. Wang, Y.-X. Yin, T.-T. Zuo, W. D., J.-Y. Li, J.-L. Shi, C.-H. Zhang, N.-W. Li, C.-J. Li and Y.-G. Guo, *Adv. Mater.,* **2017**, 1703729

26. S. Wu, Z. Zhang, M. Lan, S. Yang, J. Cheng, J. Cai, J. Shen, Y. Zhu, K. Zhang and W. Zhang, *Adv. Mater.,* **2018**, 1705830

27. L. Liu, Y.-X. Yin, J.-Y. Li, S.-H. Wang, Y.-G. Guo and L.-J. Wan, *Adv. Mater.,* **2018**, 30, 1706216

28. L.-Y. Qi, L. Shang, X. Chen, L. Ye, W. Zhang, P. Feng, W. Zou, N. Cao, H.-H. Zhou, D. A. Weitz, and X. Li, *Adv. Mater. Interfaces*., **2018**, 1800807

29. L. Liu, Y.-X. Yin, J.-Y. Li, Y.-G. Guo and L.-J. Wan, *Chem. Commun.,* **2018**, 54, 5330-5333

30. Y. Yang, J. Xiong, J. Zeng, J. Huang and J. Zhao, *Chem. Commun.*, **2018**, 54, 1178

31. S.-S. Chi, Y. Liu, W.-L. Song, L.-Z. Fan and Q. Zhang, *Adv. Funct. Mater.,* **2017**, 1700348

32. H. Wang, D. Lin, Y. Liu, Y. Li, Y. Cui, *Sci. Adv.,* **2017,** 3, e1701301

33. X. Ji, D.-Y. Liu, D. G. Prendiville, Y. Zhang, X. Liu, G. D. Stucky, *Nano Today.,* **2012**, 7, 10-20

34. Y. Liu, D. Lin, Z. Liang, J. Zhao, K. Yan and Y. Cui, *Nat. Commun.,* **2016**, 7, 10992

35. P. Zou1, Y. Wang, S.-W. Chiang, X. Wang, F. Kang and C. Yang., *Nat. Commun.,* **2018**, 9, 464

36. K. Yan1, Z. Lu, H.-W. Lee, F. Xiong, P.-C. Hsu, Y. Li, J. Zhao, S. Chu and Y. Cui, *Nat. Energy.,* **2016**, 1, 1-8

37. J. Pu, J. Li, Z. Shen, C. Zhong, J. Liu, H. Ma, J. Zhu, H. Zhang and P. V Braun, *Adv. Funct. Mater.* **2018**, 1804133

38. H. Lee, J. Song, Y.-J. Kim, J.-K. Park and H.-T. Kim, *Sci. Rep.,* **2016**, 6, 30830

39. J.-H. Kim, J.-H. Kim, E.-S. Choi, H. K. Yu, J. H. Kim, Q. Wu, S.-J. Chun, S.-Y. Lee and S.-Y. Lee, *J. Power Sources*, **2013**, 242, 533-540

40. Z. Liang, G. Zheng, C. Liu, N. Liu, W. Li, K. Yan, H. Yao, P.-C. Hsu, S. Chu and Y. Cui, *Nano Lett.,* **2015**, 15, 2910−2916

41. R. Pan, X. Xu, R. Sun, Z. Wang, J. Lindh, K. Edström, M. Strømme and L. Nyholm, *Small.,* **2018**, 1704371

42. S. Leijonmarck, A. Cornell, G¨. Lindbergh and L. W°agberg, *J. Mater. Chem. A*, **2013**, 1, 4671

43. K.-H. Choi, S.-J. Cho, S.-J. Chun, J. T. Yoo, C. K. Lee, W. Kim, Q. Wu, S.-B. Park, D.-H. Choi, S.-Y. Lee and S.-Y. Lee, *Nano Lett.,* **2014**, 14, 5677−5686

44. L.-L. Lu, J. Ge, J.-N. Yang, S.-M. Chen, H.-B. Yao, F. Zhou and S.-H. Yu, *Nano Lett.,* **2016**, 16, 4431−4437

45. C.-P. Yang, Y.-X. Yin, S.-F. Zhang, N.-W. Li and Y.-G. Guo, *Nat. Commun.,* **2015**, 6:8058

46. Q. Yun, Y.-B. He, W. Lv, Y. Zhao, B. Li, F. Kang and Q.-H. Yang, *Adv. Mater.,* **2016**, 28, 6932–6939

47. C. Zhang, S. Liu, G. Li, C. Zhang, X. Liu, and J. Luo, *Adv. Mater.,* **2018**, 30, 1801328

48. Y. Won, A. Kim, D. Lee, W. Yang, K. Woo, S. Jeong and J. Moon, *NPG Asia Mater.,* **2014**, 6, e105

49. T.-T. Zuo, X.-W. Wu, C.-P. Yang, Y.-X. Yin, H. Ye, N.-W. Li and Y.-G. Guo, *Adv. Mater.,* **2017**, 29, 1700389

50. Y. Ana, H. Fei, G. Zenga, X. Xu, L. Ci, B. Xi, S. Xiong, J. Feng, Y. Qian, *Nano Energy.,* 2018, 47, 503–511

51. W. Xue, L. Miao, L. Qie, C. Wang, S. Li, J. Wang and J. Li, *Curr. Opin. Electrochem.,* **2017**, 6, 92–99

52. X. Ke, Y. Cheng, J. Liu, L. Liu, N. Wang, J. Liu, C. Zhi, Z. Shi and Z. Guo, *ACS Appl. Mater. Interfaces.,* **2018**, 10, 13552−13561

53. H. Liua, E. Wanga, Q. Zhanga, Y. Renb, X. Guoa, L. Wanga, G. Lia, H. Yua, *Energy Storage Materials,* **2018**

54. L. Liu, Y.-X. Yin, J.-Y. Li, S.-H. Wang, Y.-G. Guo and L.-J. Wan, *Adv. Mater.,* **2018**, 30, 1706216